

Effectively one-dimensional phase diagram of CuZr liquids and glasses

Laura Friedeheim, Jeppe C. Dyre,^{*} and Nicholas P. Bailey[†]
*“Glass and Time”, IMFUFA, Dept. of Science and Environment,
 Roskilde University, P. O. Box 260, DK-4000 Roskilde, Denmark*
 (Dated: March 1, 2021)

This paper presents computer simulations of $\text{Cu}_x\text{Zr}_{100-x}$ ($x = 36, 50, 64$) in the liquid and glass phases. The simulations are based on the effective-medium theory (EMT) potentials. We find good invariance of both structure and dynamics in reduced units along the isomorphs of the systems. The state points studied involve a density variation of almost a factor of two and temperatures going from 1500 K to above 4000 K for the liquids and from 500 K to above 1500 K for the glasses. For comparison, results are presented also for similar temperature variations along isochores, showing little invariance. In general for a binary system the phase diagram has three axes: composition, temperature and pressure (or density). When isomorphs are present, there are effectively only two axes, and for a fixed composition just one. We conclude that the thermodynamic phase diagram of this metallic glass former for a fixed composition is effectively one-dimensional in the sense that many physical properties are invariant along the same curves, implying that in order to investigate the phase diagram, it is only necessary to go across these curves.

^{*} dyre@ruc.dk

[†] nbailey@ruc.dk

I. INTRODUCTION

Metallic systems constitute a very important category of glass formers due to their potential applications, as well as their suitability as model systems for studies of the glass transition in computer simulations [1–5]. A well-studied example is the CuZr system, which is a fairly good glass former despite consisting of just two elements [3, 6]. This paper presents numerical evidence that both above and below the glass transition, CuZr systems are simpler than has hitherto been recognized. Specifically, for three different compositions of the CuZr system we show that curves exist in the thermodynamic phase diagram along which the atomic structure and dynamics are invariant to a good approximation. The implication is that the two-dimensional thermodynamic phase diagram becomes effectively one-dimensional in regard to many material properties.

The background of the investigation is the following. In liquid-state theory, a simple liquid is traditionally defined as a single-component system of particles described by classical Newtonian mechanics and interacting by pair-potential forces [7–12]. It has been known for more than half a century that the hard-sphere (HS) model reproduces well the physics of many simple liquids, both in regard to the radial distribution function (RDF) and to dynamic properties such as the viscosity or the diffusion coefficient [12–18]. The traditional explanation of this is the “van der Waals picture” according to which the repulsive forces dominate the physics of simple liquids [12, 15–17, 19].

The HS model is a caricature simple liquid with pair forces that are zero except right at the particle collisions. In the HS model, temperature plays only the trivial role of determining particle velocities and thus the time scale; temperature is entirely unrelated to the geometry of particle positions. This implies that the thermodynamic phase diagram of the HS system is effectively one-dimensional with density as the only non-trivial variable: the dynamics of two different HS systems with the same packing fraction but different temperatures are identical, except for a trivial uniform scaling of the space and time coordinates. As a consequence, scaled RDFs are identical, scaled mean-square displacements are identical, viscosities are trivially related, etc.

The mapping of a simple liquid to a HS system presents the issue of identifying the effective HS packing fraction at a given thermodynamic state point of the liquid. Many suggestions have been made for how to calculate the relevant hard-sphere radius, yet no consensus was ever arrived at [20–28]. Already in 1977, Rosenfeld suggested a brilliant thermodynamics-based alternative by basically reasoning as follows [29]: Since the HS packing fraction determines the configurational part of the entropy, this quantity provides the required mapping between a simple liquid and its corresponding HS system. Defining the excess entropy S_{ex} as the system’s entropy minus that of an ideal gas at the same density and temperature [12, 29], S_{ex} quantifies the configurational entropy (note that $S_{\text{ex}} < 0$ because any system is less disordered than an ideal gas). Rosenfeld’s suggestion implies invariance of the physics along the curves of constant excess entropy in the phase diagram. He validated this from that time’s fairly primitive computer simulations of the Lennard-Jones system and a few other simple liquids [29]. Rosenfeld’s insight is now referred to as “excess-entropy scaling”, a property that has received increasing attention since the turn of the century because it has been found to apply also for many non-simple systems like liquid mixtures, molecular liquids, confined liquids, crystalline solids, etc [30].

In the same time period of the last 20 years, glass science has progressed significantly by the introduction of density scaling, also called thermodynamic scaling. This is the discovery that in the search for a simple mathematical description, the relevant thermodynamic variables are not temperature and pressure, but temperature T and the particle number density ρ [31–36]. When density scaling is applied to experimental data, if γ is the so-called density-scaling exponent, plotting data for the dynamics as a function of ρ^γ/T results in a collapse [32, 33, 35, 36]. This means that the dynamics depends on the two variables of the thermodynamic phase diagram only via the single number ρ^γ/T . It should be emphasized that density scaling is not universally applicable; for instance, it works better for van der Waals liquids and metals than for hydrogen-bonded liquids [33, 36, 37]. An important extension of density scaling was the discovery of isochronal superposition, according to which not only the average relaxation time is invariant along the curves of constant ρ^γ/T , so are the frequency-dependent response functions [38–40]. This indicates that the way atoms or molecules move about each other is identical at state points with same the same value of ρ^γ/T . One may think of this as a “same-movie” property: Filming the atoms/molecules at two such state points results in the same movie except for a uniform scaling of all particle positions and of the time.

The above-mentioned findings can all be derived from the hidden-scale-invariance property stating that the ordering of a system’s configurations $\mathbf{R} \equiv (\mathbf{r}_1, \dots, \mathbf{r}_N)$ (in which N is the number of particles and \mathbf{r}_i is the position of particle i) according to their potential energy, $U(\mathbf{R})$, at one density is maintained if the configurations are scaled uniformly to a different density [41]. The formal mathematical definition of hidden scale invariance is the following logical implication

$$U(\mathbf{R}_a) < U(\mathbf{R}_b) \Rightarrow U(\lambda \mathbf{R}_a) < U(\lambda \mathbf{R}_b). \quad (1)$$

Equation (1) implies that structure and dynamics, when given in proper reduced units, are invariant along the curves of constant excess entropy, the system’s so-called isomorphs [30, 41, 42]. This result is rigorous if Eq. (1) applies

without exception, but this is never the case for realistic models. However, isomorph invariance is still a good approximation if Eq. (1) applies for most of the physically important configurations and for scaling parameters λ relatively close to unity. This is believed to be the case for many metals and van der Waals bonded systems, whereas systems with strong directional bonds like hydrogen-bonded and covalently bonded systems are not expected to obey isomorph-theory predictions [43]. For metals, however, the existence of isomorphs has only been validated in a few cases [44, 45].

In isomorph theory the density-scaling exponent γ is generally state-point dependent. This has recently been confirmed in high-pressure experimental data [46–48]. Systems with hidden scale invariance are referred to as R-simple in order to indicate the simplification of the physics that follows from this symmetry; most, though not all, pair-potential systems are R-simple and several molecular systems are also R-simple, necessitating a specific name for this class of systems.

The purpose of the present paper is to check for isomorphs in a typical metallic glass former. For this we have chosen to study three different CuZr mixtures. The systems have been computer simulated both in the liquid and glass phases, using the effective-medium theory (EMT) interaction potential [49–51]. We find good isomorph invariance of structure and dynamics involving density changes up to a factor of two. This implies a significant simplification in the description of the physics of this metallic glass former since the thermodynamic phase diagram of CuZr is effectively one-dimensional.

II. THE EFFECTIVE-MEDIUM-THEORY POTENTIAL

The EMT potential [49–51] is one of several similar potentials aimed at describing metals with an accuracy comparable to that of a full density-functional-theory (DFT) treatment, but at a much lower computational cost. A widely used class of potentials in this group of mean-field potentials is the embedded atom method (EAM) [52, 53]. EMT and EAM both write the total energy E as a pair-potential part plus a function of the local electron density at each particle. The EMT realizes this in a semi-empirical way, whereas the parameters of the EAM are determined by fitting to experimental properties of the bulk solid. For more on the relation between the EAM and EMT potentials, the reader is referred to Refs. 49 and 50, while Ref. 51 gives a detailed derivation of the EMT potential and its parameters (see also the Appendix). A great advantage of the EMT is that the mathematical expression for the energy is relatively simple. This made it straightforward to implement EMT in our GPU-code RUMD [54], whereas the EAM typically involves tabulated data that are not easily implemented efficiently in GPU computing.

The core of the EMT potential is a well chosen reference system defining the *effective medium*. The total energy of the system is the energy of the reference system plus the difference to the real system. Thus the EMT total energy is written

$$E = \sum_i E_{c,i} + \left(E - \sum_i E_{c,i} \right) \quad (2)$$

where $E_{c,i}$ is the so-called cohesive energy, which is the energy of atom i in the reference system. The idea is now that the difference term should be small enough to be treated accurately by first-order perturbation theory. To obtain this the reference system must be as close as possible to the real system.

The real and the reference systems are linked by a “tuning parameter”. In the first version of the EMT potential, the homogeneous electron gas was used as the reference system, with the electron density as the tuning parameter [55, 56]. The EMT version used in this paper is that of Ref. 51 for which a perfect fcc crystal is the reference system. Here, the lattice constant serves as the tuning parameter, i.e., is used to adjust the environment of an atom such that the average electron density surrounding the atom matches that of the real system.

The EMT potential of a pure metal involves seven parameters: the negative cohesive energy E_0 , a charge density parameter n_0 , the Wigner-Seitz radius s_0 (defined in terms of the atomic, not the electronic density), a parameter η quantifying the influence of the density tail surrounding an neighboring atom, a parameter λ determined from the bulk modulus, and finally the product $V_0(\beta\eta_2 - \kappa)$ determined from the shear modulus. The density-related parameters n_0 and η were originally calculated self-consistently by reference to the homogeneous electron gas, while the five other parameters are determined from experimental or *ab initio* data. More details on how the parameters are determined for single and compound systems can be found in the Appendix and in Refs. 55 and 57. The parameter values for CuZr used in this work are those of Ref. 57, where parameters were adjusted to match DFT-determined properties—cohesive energies, lattice constants and elastic constants—of both the pure metals and a Cu₅₀Zr₅₀ alloy structure.

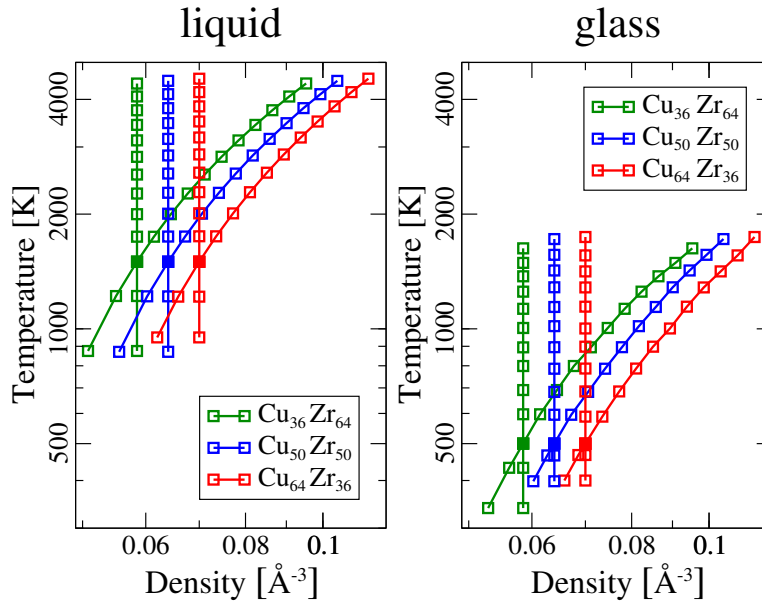


FIG. 1. Logarithmic density-temperature phase diagrams showing all state points simulated along isochores (vertical lines) and isomorphs (lines at an angle). The colors reflect the three different compositions studied. The left figure gives liquid state points, the right figure gives glass state points. Each isomorph is generated by means of the direct-isomorph-check method (see the text), proceeding in steps of 5% density changes starting from “reference” state points at temperature 1500 K for the liquids and 500 K for the glasses (full symbols). The reference state point densities were selected to have approximately the same pressure (~ 17 GPa), while the lowest-density state points have approximately zero pressure (compare Tables I and II). The isochores studied below for comparison to the isomorphs are the vertical lines through each reference state point.

III. REDUCED QUANTITIES

Structure and dynamics are invariant along isomorphs only when these are given in so-called reduced versions based on a “macroscopic” unit system that depends on the state point in question. The unit system defining reduced variables reflects the system’s volume V and temperature T as follows. If the particle number density is $\rho \equiv N/V$, the length, energy, and time units are, respectively, [42]

$$l_0 = \rho^{-1/3}, \quad e_0 = k_B T, \quad t_0 = \rho^{-1/3} \sqrt{\frac{m}{k_B T}}. \quad (3)$$

Here m is the average particle mass. Equation (3) refers to Newtonian dynamics; for Brownian dynamics one uses the same length and energy units, but a different time unit [42]. All physical quantities can be made dimensionless by reference to the above units. “Reduced” quantities are denoted by a tilde, for instance

$$\tilde{\mathbf{R}} \equiv \rho^{1/3} \mathbf{R}. \quad (4)$$

IV. TRACING OUT ISOMORPHIC STATE POINTS

Three compositions were studied, $\text{Cu}_{36}\text{Zr}_{64}$, $\text{Cu}_{50}\text{Zr}_{50}$, and $\text{Cu}_{64}\text{Zr}_{36}$. Figure 1 presents the state points simulated in a density-temperature thermodynamic phase diagram. Isomorph invariance is never perfect in realistic systems. In order to estimate to which degree this invariance holds, it is therefore useful to compare structure and dynamics variations along isomorphs to what happens along curves of similar temperature or density variation, which are not isomorphs. We have chosen to compare to isochores (lines of constant density) with the same temperature variation as the isomorphs. The isochores, of course, are the vertical straight lines in Fig. 1, the isomorphs are the lines with a slope. The high-temperature state points describe equilibrium liquids, the low-temperature points are glass-phase state points.

We now turn to the challenge of tracing out isomorphs. Recall that an isomorph is a curve of constant S_{ex} for a system that obeys the hidden-scale-invariance condition Eq. (1) at the relevant state points. To which degree this condition is obeyed may be difficult to judge because Eq. (1) always applies when λ is close to unity, but fortunately a practical criterion exists: Eq. (1) applies to a good approximation if and only if the virial W and potential energy U are strongly correlated in their thermal-equilibrium constant-density (NVT) fluctuations [41]. These fluctuations are characterized by the Pearson correlation coefficient R defined by (in which sharp brackets denote canonical-ensemble averages and Δ is the deviation from the thermal average)

$$R = \frac{\langle \Delta U \Delta W \rangle}{\sqrt{\langle (\Delta U)^2 \rangle \langle (\Delta W)^2 \rangle}}. \quad (5)$$

As a pragmatic criterion, $R > 0.9$ is usually used for delimiting where isomorph-theory predictions are expected to apply [42, 43, 58]. For the CuZr systems we find that R goes below 0.9 at high densities in the liquid phase, as well as in most of the glass phase (Fig. 2), but at most state points studied R is above 0.8. Thus it makes good sense to test for isomorph invariance.

Tracing out a curve of constants excess entropy is straightforward if one knows how S_{ex} varies throughout the phase diagram. It is a bit challenging to evaluate entropy, however, because this involves thermodynamic integration (or the Widom insertion method that is also tedious). In order to trace out an isomorph, one does not need to know the value of S_{ex} , however, and one can therefore make use of the following general identity

$$\gamma \equiv \left(\frac{\partial \ln T}{\partial \ln n} \right)_{S_{\text{ex}}} = \frac{\langle \Delta U \Delta W \rangle}{\langle (\Delta U)^2 \rangle}. \quad (6)$$

Here the quantity γ is the (state-point dependent) density-scaling exponent defined as the isomorph slope in a logarithmic density-temperature phase diagram like that of Fig. 1. The second equality sign is a statistical-mechanical identity that allows for calculating γ from NVT equilibrium fluctuations at the state point in question [42]. Figure 2 shows how γ varies along the isomorphs of the CuZr systems studied below, plotted as a function of the density relative to that of the isomorph reference state point. All cases show similar behavior with γ decreasing significantly with increasing density. This indicates a softening of the interactions at high densities.

Equation (6) can be used to trace out an isomorph by numerical integration, for instance using the Euler algorithm for small density changes of order one percent [42] or using the fourth-order Runge-Kutta algorithm that allows for significantly larger density changes [59]. Both methods are fool proof, but involve many simulations if one wishes to cover a significant density range. There are alternative “quick and dirty” methods which, depending on the system in question, can be quite useful. For instance, isomorphs of the Lennard-Jones system are to a good approximation given by $h(\rho)/T = \text{Const.}$ in which $h(\rho) = (\gamma_0/2 - 1)(\rho/\rho_0)^4 - (\gamma_0/2 - 2)(\rho/\rho_0)^2$ in which γ_0 is the density-scaling exponent at a selected “reference state point” of density ρ_0 [60, 61].

A general and fairly efficient method for tracing out isomorphs is the “direct isomorph check” (DIC) [42], and we used this for generating the CuZr isomorphs. The DIC is justified as follows [41]. Hidden scale invariance (Eq. (1)) implies that the microscopic excess entropy function $S_{\text{ex}}(\mathbf{R})$ is scale invariant, i.e., a function only of a configuration’s reduced coordinate $\tilde{\mathbf{R}}$: $S_{\text{ex}}(\mathbf{R}) = S_{\text{ex}}(\tilde{\mathbf{R}})$ [41]. From the definition of $S_{\text{ex}}(\mathbf{R})$ it follows that $U(\mathbf{R}) = U(\rho, S_{\text{ex}}(\tilde{\mathbf{R}}))$ in which the function $U(\rho, S_{\text{ex}})$ is the average potential energy at the state point with density ρ and excess entropy S_{ex} [41]. Considering configurations with the same density ρ and small deviations in the microscopic excess entropy from that of the given state point S_{ex} , an expansion to first order leads to

$$U(\mathbf{R}) \cong U(\rho, S_{\text{ex}}) + T(\rho, S_{\text{ex}}) \left(S_{\text{ex}}(\tilde{\mathbf{R}}) - S_{\text{ex}} \right). \quad (7)$$

Consider two state points (ρ_1, T_1) and (ρ_2, T_2) with the same excess entropy S_{ex} and average potential energies U_1 and U_2 , respectively. If \mathbf{R}_1 and \mathbf{R}_2 are configurations of these state points with the same reduced coordinates, i.e., obeying

$$\rho_1^{1/3} \mathbf{R}_1 = \rho_2^{1/3} \mathbf{R}_2 \equiv \tilde{\mathbf{R}}, \quad (8)$$

one gets by elimination of the common factor $S_{\text{ex}}(\tilde{\mathbf{R}}) - S_{\text{ex}}$ in Eq. (7) with $T_1 \equiv T(\rho_1, S_{\text{ex}})$ and $T_2 \equiv T(\rho_2, S_{\text{ex}})$

$$\frac{U(\mathbf{R}_1) - U_1}{T_1} \cong \frac{U(\mathbf{R}_2) - U_2}{T_2}. \quad (9)$$

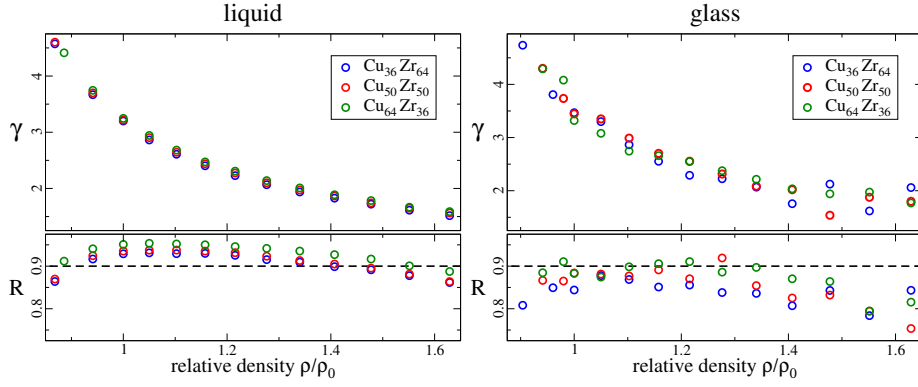


FIG. 2. Virial potential-energy Pearson correlation coefficient R (Eq. (5)) and density-scaling exponent γ (Eq. (6)), plotted along the isomorphs as a function of the density relative to that of the reference state point (which has temperature 1500 K for liquids and 500 K for glasses). The left figure is the liquid, the right figure is the glass. We see similar pictures in the two cases, with γ decreasing significantly as density is increased, indicating an effective softening of the interactions. The virial potential-energy correlations are generally strong, with a maximum at densities close to the reference state point densities denoted by ρ_0 . The dashed lines mark $R = 0.9$, which is traditionally used for delimiting state points for which isomorph-theory predictions are expected to apply [42, 58].

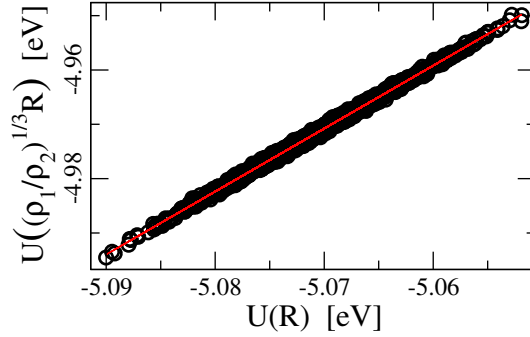


FIG. 3. Example of a direct isomorph check (DIC), here with state point 1 being the reference state point of the 64-36 mixture ($T = 1500\text{K}$) and state point 2 having a 5% higher density. At state point 1, a series of thermal-equilibrium configurations \mathbf{R} are sampled. Each of these are scaled uniformly by the factor $(\rho_2/\rho_1)^{-1/3} = 0.9839$, resulting in a scaling to a 5% higher density. Plotting the potential energy of scaled versus unscaled configuration, the slope of the best fit line is T_2/T_1 , compare Eq. (10); this determines the temperature T_2 that makes the state point (ρ_2, T_2) isomorphic to state point (ρ_1, T_1) .

While not of direct relevance for the present paper, we note that Eq. (9) implies $\exp(-U(\mathbf{R}_1)/k_B T_1) \propto \exp(-U(\mathbf{R}_2)/k_B T_2)$, i.e., that the two configurations have the same canonical probability. This is a manifestation of the hidden scale invariance inherent in isomorph theory [42]. Equation (9) leads to $U(\mathbf{R}_2) \cong (T_2/T_1)U(\mathbf{R}_1) + (U_2 - (T_2/T_1)U_1)$. For the fluctuations about the respective mean values this implies

$$\Delta U(\mathbf{R}_2) \cong \frac{T_2}{T_1} \Delta U(\mathbf{R}_1). \quad (10)$$

Equation (10) implies that isomorphic state points may be identified as follows: First sample a set of equilibrium configurations at the state point (ρ_1, T_1) . Then scale these configurations uniformly to density ρ_2 . The temperature T_2 of the state point with density ρ_2 , which is isomorphic to state point (ρ_1, T_1) , is now found from the slope of a scatter plot of the potential energies of scaled versus unscaled configurations. An example of how this works is shown in Fig. 3.

Because the hidden-scale-invariance property is not exact, the DIC is less reliable for large density changes than for smaller ones. We traced out the isomorphs studied below using step-by-step DICs involving density changes of 5%. The resulting isomorphs are shown in Fig. 1. The simulated isomorphic state points are listed in Table I (liquid) and Table II (glass).

T [K]	ρ [\AA^{-3}]	p [GPa]	T [K]	ρ [\AA^{-3}]	P [GPa]	T [K]	ρ [\AA^{-3}]	P [GPa]
875	0.0508	1.7	870	0.0556	0.8	950	0.0620	1.5
1219	0.0551	9.6	1217	0.0602	9.0	1215	0.0659	8.4
1500	0.0585	17.2	1500	0.0640	17.2	1500	0.0700	17.1
1745	0.0614	24.6	1747	0.0672	25.2	1749	0.0735	25.6
1999	0.0645	33.2	2005	0.0706	34.5	2009	0.0772	35.7
2266	0.0677	43.2	2274	0.0741	45.4	2283	0.0810	47.6
2540	0.0711	54.8	2555	0.0778	58.0	2568	0.0851	61.3
2828	0.0747	68.0	2850	0.0817	72.5	2867	0.0893	77.3
3122	0.0784	83.0	3151	0.0858	89.2	3177	0.0938	95.6
3428	0.0823	100.1	3464	0.0901	108.1	3499	0.0985	116.6
3746	0.0864	119.5	3795	0.0946	129.7	3834	0.1034	140.7
4070	0.0908	141.3	4128	0.0993	154.2	4179	0.1086	168.0
4404	0.0953	165.8	4473	0.1042	181.8	4533	0.1140	199.0

TABLE I. Temperature, density, and pressure of liquid isomorph state points. The vertical lines divide the compositions in the following order: $\text{Cu}_{36}\text{Zr}_{64}$, $\text{Cu}_{50}\text{Zr}_{50}$, $\text{Cu}_{64}\text{Zr}_{36}$. The boldface row represents the reference state point for the isomorph of each composition.

T [K]	ρ [\AA^{-3}]	p [GPa]	T [K]	ρ [\AA^{-3}]	P [GPa]	T [K]	ρ [\AA^{-3}]	P [GPa]
339	0.0529	0.4	398	0.0602	3.1	400	0.0659	1.7
432	0.0562	6.2	466	0.0627	7.7	467	0.0686	6.6
500	0.0585	11.0	500	0.0640	10.3	500	0.0700	9.5
587	0.0614	17.6	575	0.0672	17.3	578	0.0735	17.1
683	0.0645	25.5	672	0.0706	25.9	667	0.0772	26.1
781	0.0677	34.6	773	0.0741	35.8	758	0.0810	36.8
880	0.0711	45.2	877	0.0778	47.5	858	0.0851	49.4
980	0.0747	57.6	989	0.0817	60.7	968	0.0893	64.1
1088	0.0784	71.5	1103	0.0858	76.4	1083	0.0938	81.0
1200	0.0823	87.6	1218	0.0901	94.1	1203	0.0985	100.6
1304	0.0864	105.9	1340	0.0946	114.3	1325	0.1034	123.4
1442	0.0908	126.5	1440	0.0993	137.7	1453	0.1086	149.1
1558	0.0953	149.7	1575	0.1042	163.5	1596	0.1140	178.7

TABLE II. Temperature, density, and pressure of glass isomorph state points. The vertical lines divide the compositions shown in the following order: $\text{Cu}_{36}\text{Zr}_{64}$, $\text{Cu}_{50}\text{Zr}_{50}$, $\text{Cu}_{64}\text{Zr}_{36}$. The boldface row represents the reference state point for the isomorph of each composition. The starting point for the glass isomorph is at the same density as the liquid isomorph starting point, but with temperature 500K.

V. SIMULATION DETAILS

The three compositions studied in this work are $\text{Cu}_x\text{Zr}_{100-x}$ ($x = 36, 50, 64$). For each of these an isomorph was generated from a state point well into the liquid regime. From this initial “reference” state point at temperature 1500 K, an isomorph was traced out using the DIC as described above. The majority of state points are at a higher density than that of the reference state point, ρ_0 , but for each isomorph we also generated two isomorph state points at lower densities to ensure that samples close to zero pressure were included in the study (compare Tables I and II).

For each state point on an isomorph, a state point was simulated at the same temperature at the reference-state-point density; these constitute the isochoric state points discussed below along with the isomorph state points. For all three compositions, the glass-phase reference state points were obtained by cooling at a constant rate in 100000 time steps from the liquid reference state point at 1500 K to the glass isomorph reference temperature 500 K. This is a high cooling rate, corresponding roughly to 1 K/ps.

From these three glass reference state points, isomorphs were generated by the DIC method in the same way as for the liquids.

The simulations were carried out in RUMD [54], Roskilde university’s GPU Molecular Dynamics package that is

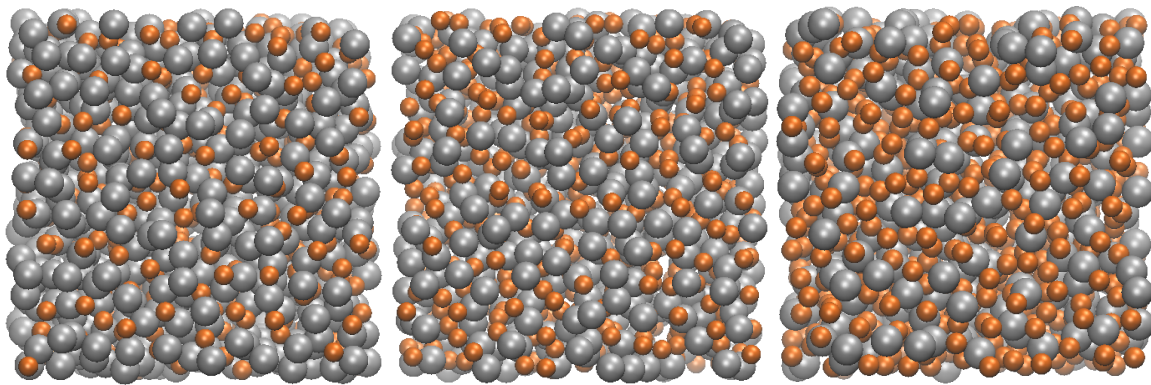


FIG. 4. Snapshots of the glass configurations at the glass isomorph reference state points at 500 K. The Cu atoms are orange, the Zr atoms are grey. From left the figures are for the 36-64, 50-50, and 64-36 CuZr compositions.

optimized for small systems. The NVT ensemble was used to simulate cubic boxes containing 1000 particles. The initial configuration was a simple cubic crystal with particle types assigned randomly at the required ratios. At each state point of the liquid, 10^4 MD steps of equilibration were performed to melt and equilibrate the liquid. Following this we carried out 10^6 MD steps of the production run. For the glass-phase simulations, 10^5 MD steps of equilibration were performed before 10^7 MD steps of the production run. The time step in the simulations was $0.5 \text{ \AA}^{1/2}(\text{u/eV})^{1/2}$ in which u is the atomic mass.

Figure 4 shows the glasses prepared by cooling the liquids to the glass-isomorph reference state points. There are no signs of crystallization.

VI. STRUCTURE AND DYNAMICS IN THE LIQUID PHASE

To investigate how the structure varies along isomorphs and isochores for the three CuZr compositions we probed the radial distribution functions (RDFs), which in reduced units are predicted to be isomorph invariant. There are three different RDFs, one for Cu-Cu, one for Cu-Zr, and one for Zr-Zr. Plotting a RDF in reduced units implies scaling the distance variable according to the density (compare Eq. (4)). This results in peaks at roughly the same places for all compositions because the scaling corresponds to taking the system to unit density.

Figure 5 shows the reduced RDFs along the isomorphs and Fig. 6 shows the similar RDFs along isochores with same temperature variation (compare Fig. 1 showing the similar state points). Comparing the two, we conclude that the structure is isomorph invariant to a good approximation, but varies significantly along the isochores. Deviations are largest for the minority-minority RDFs for the non-equi-molar compositions. Deviations from isomorph invariance are also seen in some cases at the first maximum, where the maximum is generally lowered somewhat with increasing density. This is an effect that is well understood for pair-particle systems, for which it derives from the fact that a higher density-scaling exponent γ implies a steeper effective pair potential and therefore less likely particle close encounters. This results in moving some of the low distance RDF to higher distances when γ is large, which is the case at low densities. This explanation suggests that γ of the present non-pair-potential simulations can also be interpreted as an effective pair IPL exponent [44]. – For the isochores, there is a general “damping” of the RDFs at all distances as temperature increases. This reflects the stronger thermal fluctuations at high temperatures.

Focusing on the height of the first RDF peak, Fig. 7 shows these for all the data of Fig. 5 and Fig. 6. The full symbols are the peak heights along the three isomorphs, whereas the open symbols are the peak heights along the corresponding isochores. Clearly, the variation is significantly larger along the isochores.

Next we investigated the dynamics. Figure 8 shows results for the reduced-unit mean-square displacement (MSD) along isomorphs and isochores, respectively (two left columns). We focus on the majority atom MSD, but found that data for the minority atom are entirely similar (not shown). Clearly, the MSD is isomorph invariant and varies significantly along the isochores. Note that the short-time ballistic-region collapse seen in all cases follows from the definition of reduced units, i.e., this collapse applies throughout the phase diagram of any system. The two right-hand columns of Fig. 8 show similar data for the incoherent intermediate scattering function (evaluated at the wave vector $2\pi\rho^{1/3}$ that is constant in reduced units). Again, isomorph invariance is clearly demonstrated.

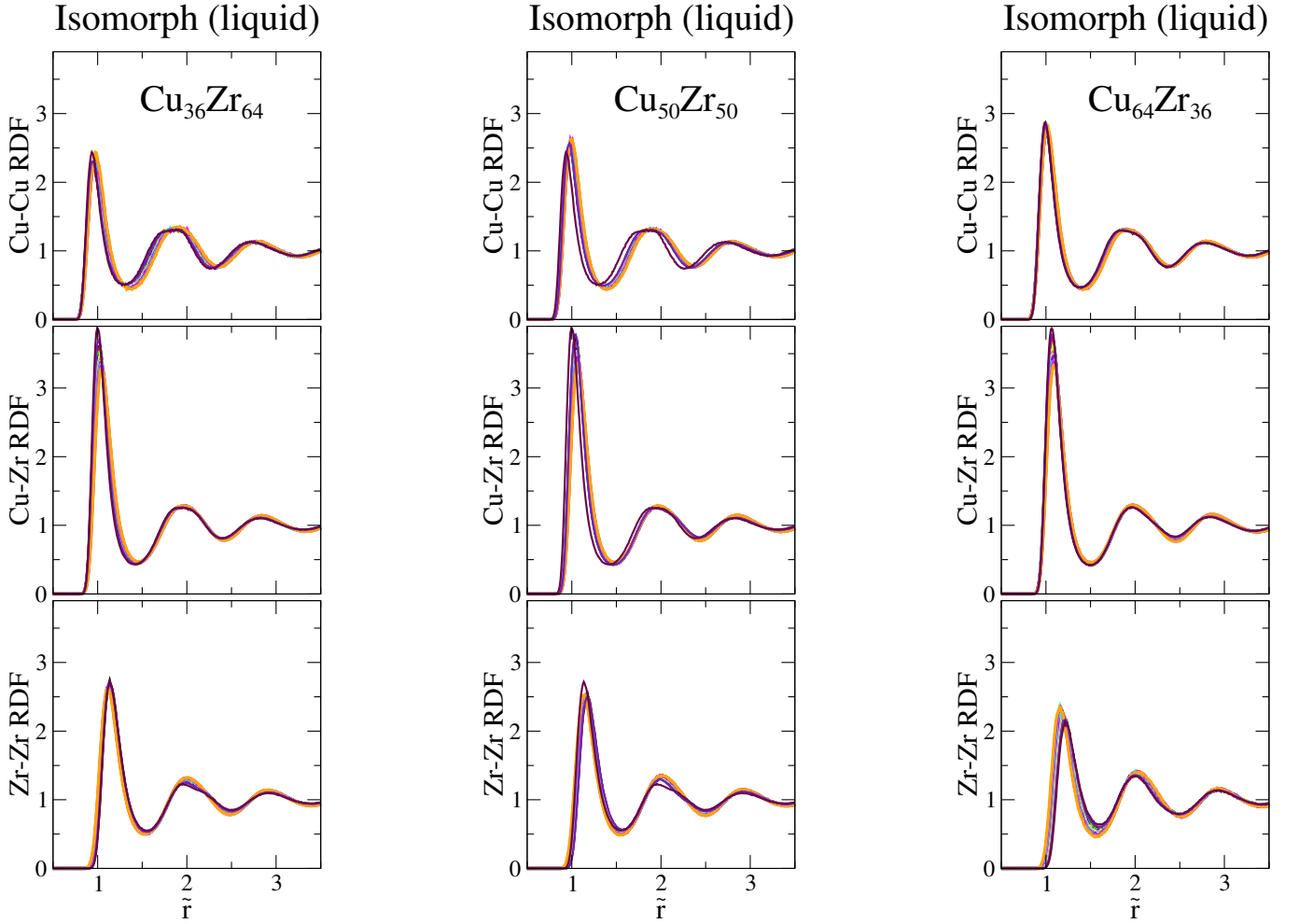


FIG. 5. Isomorph liquid-state radial distribution functions (RDFs), plotted as a function of the reduced pair distance $\tilde{r} \equiv \rho^{1/3}r$. Each column gives reduced-unit RDFs along an isomorph of one composition. The color coding used is the xmgrace default ordering with black for the data set corresponding to the reference state point, then at increasing density: red, green, blue, yellow, etc; orange is the color given to the 11th data set which is here that the highest temperature. The two state points with lower density than that of the reference state point are purple and brown. Generally, we see good approximate isomorph invariance, with some deviation at the first peak maximum and the largest overall deviations at the lowest densities (at which the virial potential-energy correlation coefficient drops rapidly, compare Fig. 2).

VII. STRUCTURE AND DYNAMICS IN THE GLASS PHASE

The above investigation was repeated in the glass phase of the three mixtures. Isomorph theory is traditionally formulated by reference to thermal equilibrium [41–43], but we ignored this and proceeded pragmatically as if a glass were an equilibrium system. Each of the three glasses were prepared by cooling with a constant rate from a configuration at the reference state point ($T = 1500\text{K}$) to temperature 500 K. For each composition, once a glass configuration was obtained at the reference state point, we generated an isomorph in the same way as the liquid isomorphs by repeated DICs involving 5% density changes. Again, for comparison we probed the RDF and the dynamics also at isochoric state points with the same temperature variation as that of the isomorphs (compare Fig. 1).

The RDFs are shown in Fig. 9 (isomorphs) and in Fig. 10 (isochores). The picture is similar to that of the liquid phase: overall, good invariance along the isomorphs is seen in contrast to a substantially larger variation along the isochores. This is also the conclusion from Fig. 11 showing all the first-peak heights as a function of the temperature.

The dynamics of the glasses is investigated via the MSD and the incoherent intermediate structure factor in Fig. 12. A glass consists mostly of atoms frozen at fixed positions, merely vibrating there. Thus the MSD is virtually constant, though some particle motion is discernible at the longest times. This “glass flow” motion does not appear to

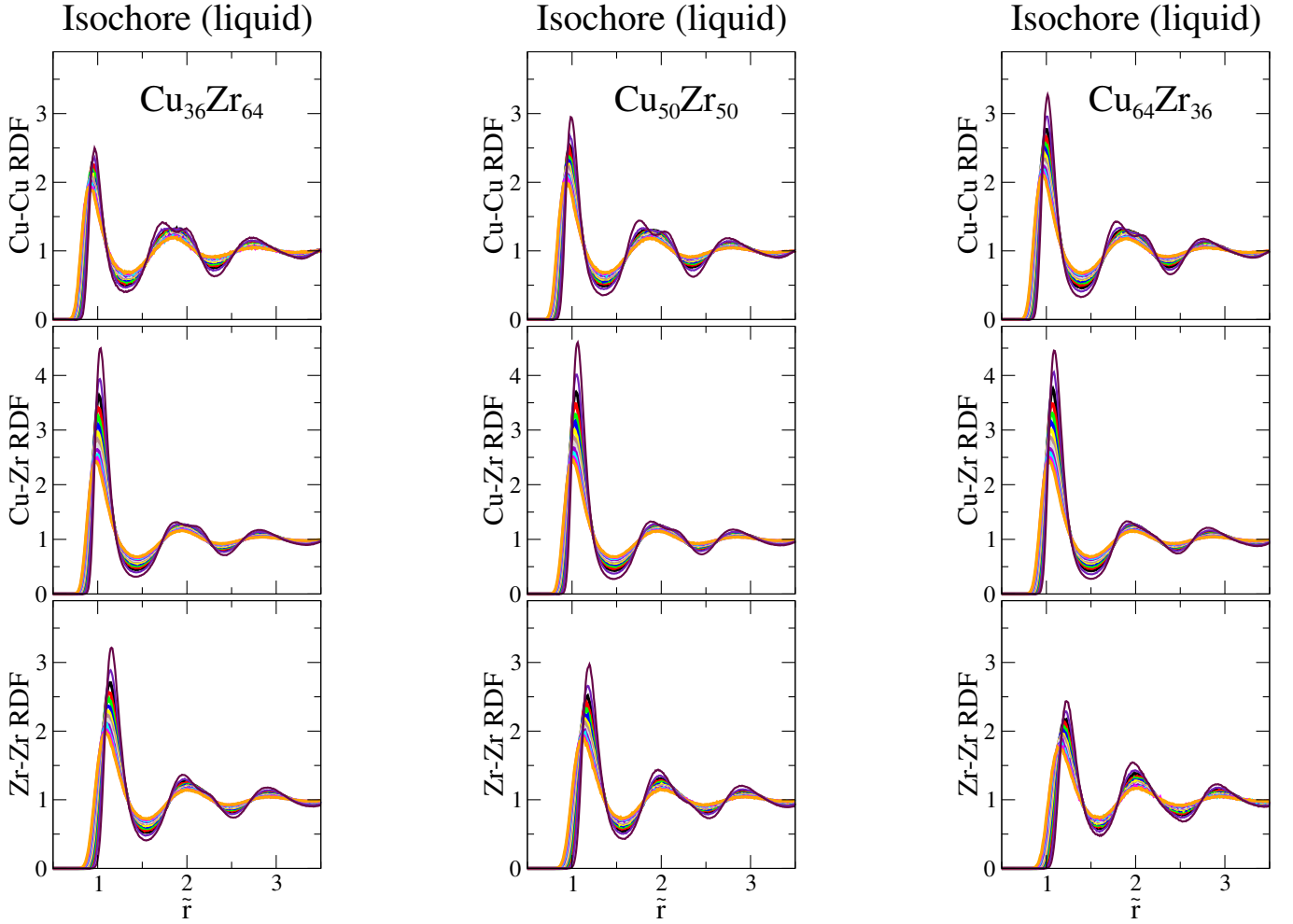


FIG. 6. Isochore liquid-state RDFs plotted as in Fig. 5. There is a considerably larger variation of the structure, with the structure being more washed out, the higher the temperature is. This reflects the increasing thermal fluctuations, which in the case of an isomorph are compensated by increasing forces (Fig. 5).

be isomorph invariant, but we found no systematic variation with the density. This indicates that the non-invariance reflects statistical uncertainty. Along the isochores (second column), it is clear that the glass gradually melts as temperature is increased when moving from the black curve representing the 500 K reference state point. The fact that the particles in the glass virtually do not move except for vibrations is also visible in the incoherent intermediate scattering function (right two columns of Fig. 12), which along the isomorphs stabilize at a constant level at long times. In contrast, many of the isochore curves go to zero at long times, reflecting an ease of motion with increasing temperature that is not achieved along the isomorphs.

VIII. SUMMARY

This paper has studied three different compositions of the CuZr system by computer simulations using the efficient EMT potentials. We have traced out isomorphs in the liquid and glass phases of the three systems. Good isomorph invariance was observed of structure and dynamics in both phases, showing that the atoms move about each other in much the same way at state points on the same isomorph. This means that the thermodynamic phase diagram of CuZr systems is effectively one-dimensional. Thus for many purposes, in order to get an overview of the CuZr system, it is enough to investigate state points belonging to different isomorphs. It should be noted, though, that some quantities like, e.g., the bulk modulus is not isomorph invariant even when given in reduced units [62]. On the other hand, most material quantities *are* isomorph invariant in reduced units, e.g., the shear modulus, the shear viscosity, the heat conductivity, etc [62].

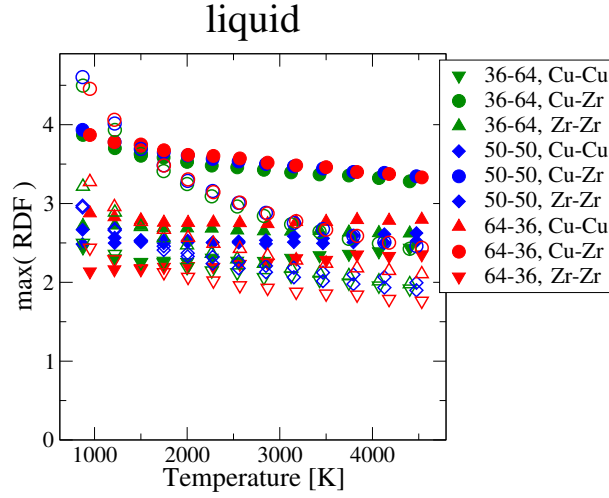


FIG. 7. Maximum values of all RDFs of Fig. 5 and Fig. 6, i.e., values of the RDFs at their first peak. The full symbols represent isomorphs and the open symbols represent isochores. While the isomorph values are not invariant, in particular for the Cu-Zr RDFs, the general picture is that of a visibly better invariance along the isomorphs than along isochores of the same temperature variation.

It would be interesting to confirm the above results using the EAM potentials. Given that the EAM and EMT both have been shown to nicely reproduce metal properties, we do not expect significantly different results. Indeed, the fact that isomorph theory describes metals well has been validated in DFT simulations of crystals [44].

ACKNOWLEDGMENTS

This work was supported by the VILLUM Foundation's *Matter* grant (16515).

APPENDIX: MORE ON THE EMT

Jacobsen, Nørskov, and Puska [51] and Puska *et al.* [49] discussed the ansatz used in the EAM with arguments based on the effective-medium approach. Jacobsen *et al.* demonstrated how the cohesive energy of a metallic system could be related to the embedding energies, with corrections accounting for the d-d hybridization in the transition metals. Their approach showed that with the neglect of the d-d hybridization (valid for simple metals and presumably for early and late transition metals), the EAM expression is recovered. For Al and Cu, for example, the practical application of the effective-medium theory is mathematically equivalent to the EAM. The density of the effective medium was taken to be an unweighted average of the background electron number density over the Wigner-Seitz cell of the atom.

As mentioned in Sec. II, the EMT potential is defined in terms of seven parameters: E_0 the negative of the cohesive energy, an electron density parameter n_0 , the Wigner-Seitz radius s_0 defined from the atomic density, η quantifying the influence of the density tail surrounding an neighboring atom, λ determined from the bulk modulus, and the product of parameters $V_0(\beta\eta_2 - \kappa)$ determined from the shear modulus. The following summarizes the discussion given in Ref. 51 on how the values for these parameters are obtained for a system with an ideal fcc crystal as reference system.

DFT shows that the correction term is a sum of atomic-sphere and one-electron corrections. The former term corrects for the difference in electrostatic and exchange-correlation energies between real and reference system. This is approximately equal to the difference in pair interactions of the two systems. The one-electron correction is given by the difference of sums over one-electron energies. This contribution does not require any fitting input from experiments and can be calculated fully *ab initio* [63]. While this would yield an accuracy comparable to that of DFT, it is also similarly computationally expensive. To circumvent this, the one-electron contribution is momentarily neglected. Including only the cohesive and the atomic-sphere correction parts, the total energy expression can be simplified to

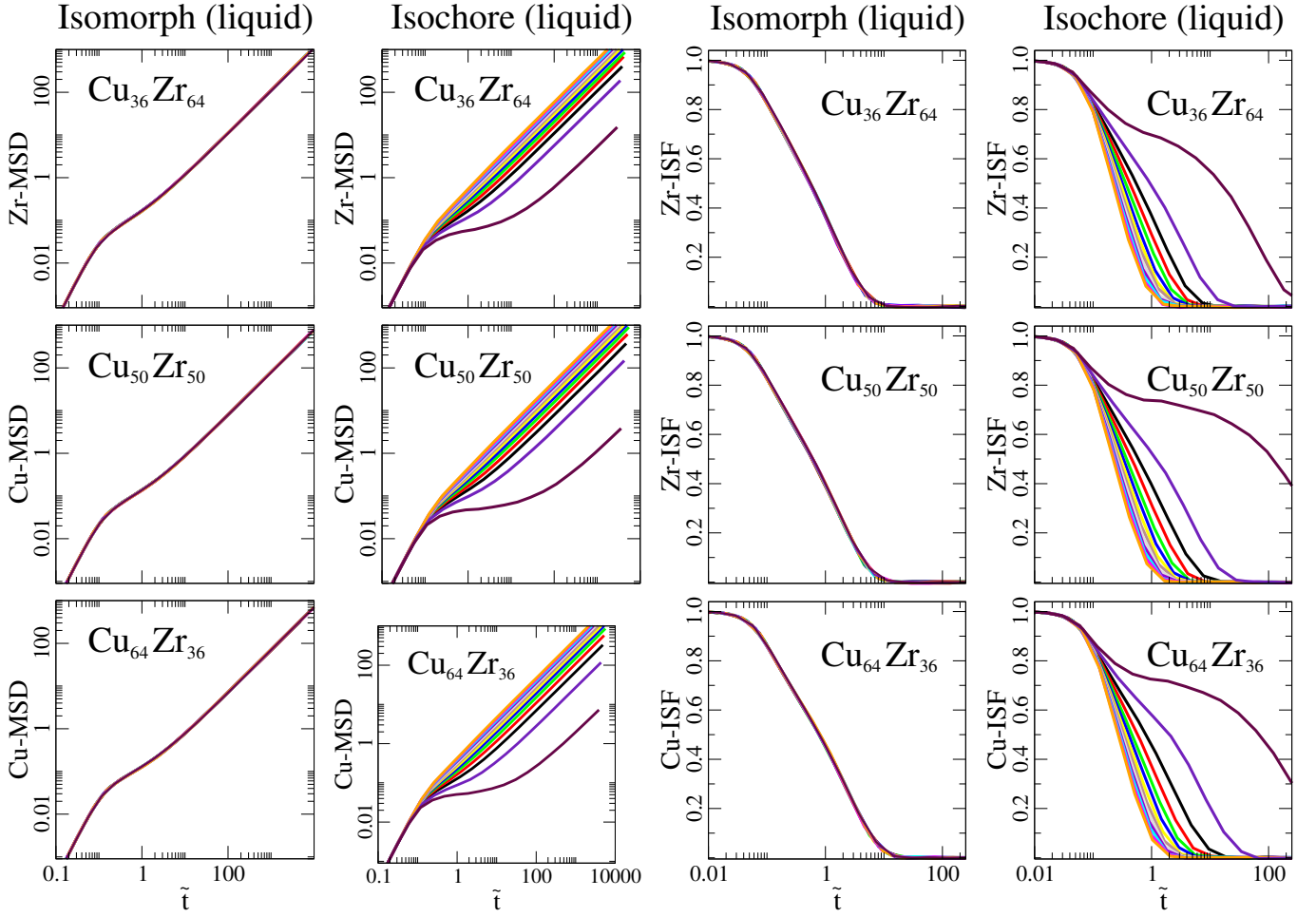


FIG. 8. Dynamics along the isomorphs and isochores of the liquids. The two left columns give data for the reduced MSD as a function of the reduced time. The two right columns give the analogous reduced-unit intermediate incoherent scattering function, for simplicity evaluated at the same wave vector in all three cases $2\pi\rho^{1/3}$, which is constant in reduced units. There is good isomorph invariance of the dynamics, but a significant variation along the isochores (except in the short-time ballistic region where the reduced MSD by definition is $3\tilde{t}^2$ at all state points).

$$\begin{aligned}
 E &= \sum_i \left(E_{c,i} + \Delta E_{AS}(i) \right) \\
 &= \sum_i \left(E_{c,i}(n_i) + \frac{1}{2} \left[\sum_{i \neq j} V_{ij}(r_{ij}) - \sum_{i \neq j}^{ref} V_{ij}(r_{ij}) \right] \right). \quad (11)
 \end{aligned}$$

Here the atomic-sphere correction term $\Delta E_{AS}(i)$ is expressed as the difference between pair potentials V_{ij} of the real and the reference system. The neglected one-electron contribution is not necessarily small enough to be neglected, but it is possible to include this contribution as a small adjustment to the potential V_{ij} .

The density argument of the cohesive energy $E_{c,i}$ is the parameter that connects the environment around a given atom i in the real system with the reference system. This so-called embedding density, n_i , is a sum of contributions from the neighboring atoms,

$$n_i = \sum_{i \neq j} \Delta n_j(s_i, r_{ij}) \quad (12)$$

in which the density “tail” $\Delta n_j(s_i, r_{ij})$ is assumed to have the following exponential form

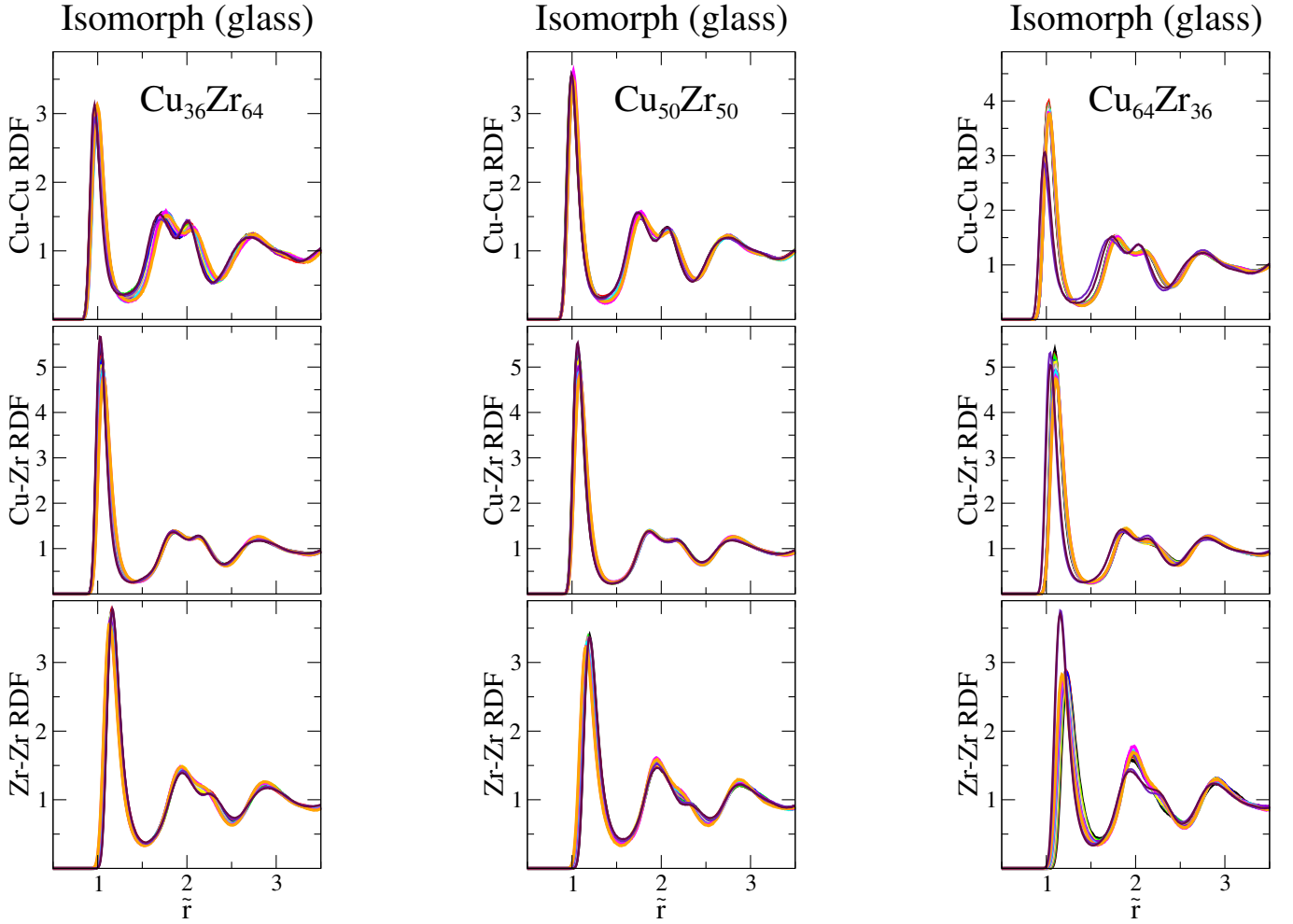


FIG. 9. Isomorph glass-state RDFs, plotted as a function of the reduced pair distance \tilde{r} . The picture is pretty much as for the liquid, with good isomorph invariance except for the somewhat more noisy data that are presumably due to the fact that, basically, only a single configuration and its vibrations is probed. Significant deviations from isomorph invariance are observed, though, for the 64% Cu mixture, both at the highest densities for the Cu-Cu RDF and at the lowest densities for the Zr-Zr RDF.

$$\Delta n(s_i, r_{ij}) = \Delta n_0 \exp [\eta_1(s_i - s_0) - \eta_2(r_{ij} - \beta s_0)]. \quad (13)$$

Here s_0 is the equilibrium Wigner-Seitz radius, s_i is the neutral sphere radius at non-zero pressure, and β is a geometric factor related to the nearest-neighbor distance d_{nn} via $\beta s = d_{nn}$ (meaning that $\beta = (16\pi/3)^{1/3}/\sqrt{2} \approx 1.81$).

Using a fcc lattice as the reference system, the atomic sphere correction can be expressed as

$$\Delta E_{AS}(i) = \frac{1}{2} \left[\sum_{j \neq i} v(r_{ij}) - 12v(\beta s_i) \right] \quad (14)$$

where the second term corresponds to the fcc lattice having 12 nearest neighbors at distance $r = \beta s_i$. The potential is given by

$$v(r) = -V_0 \exp \left(-\frac{\kappa}{\beta} (r_{ij} - \beta s_0) \right). \quad (15)$$

Input from experiments is required to determine the remaining parameters describing the elastic and structural properties of the metal in question. The cohesive energy and the parameter λ are related to the bulk modulus B via

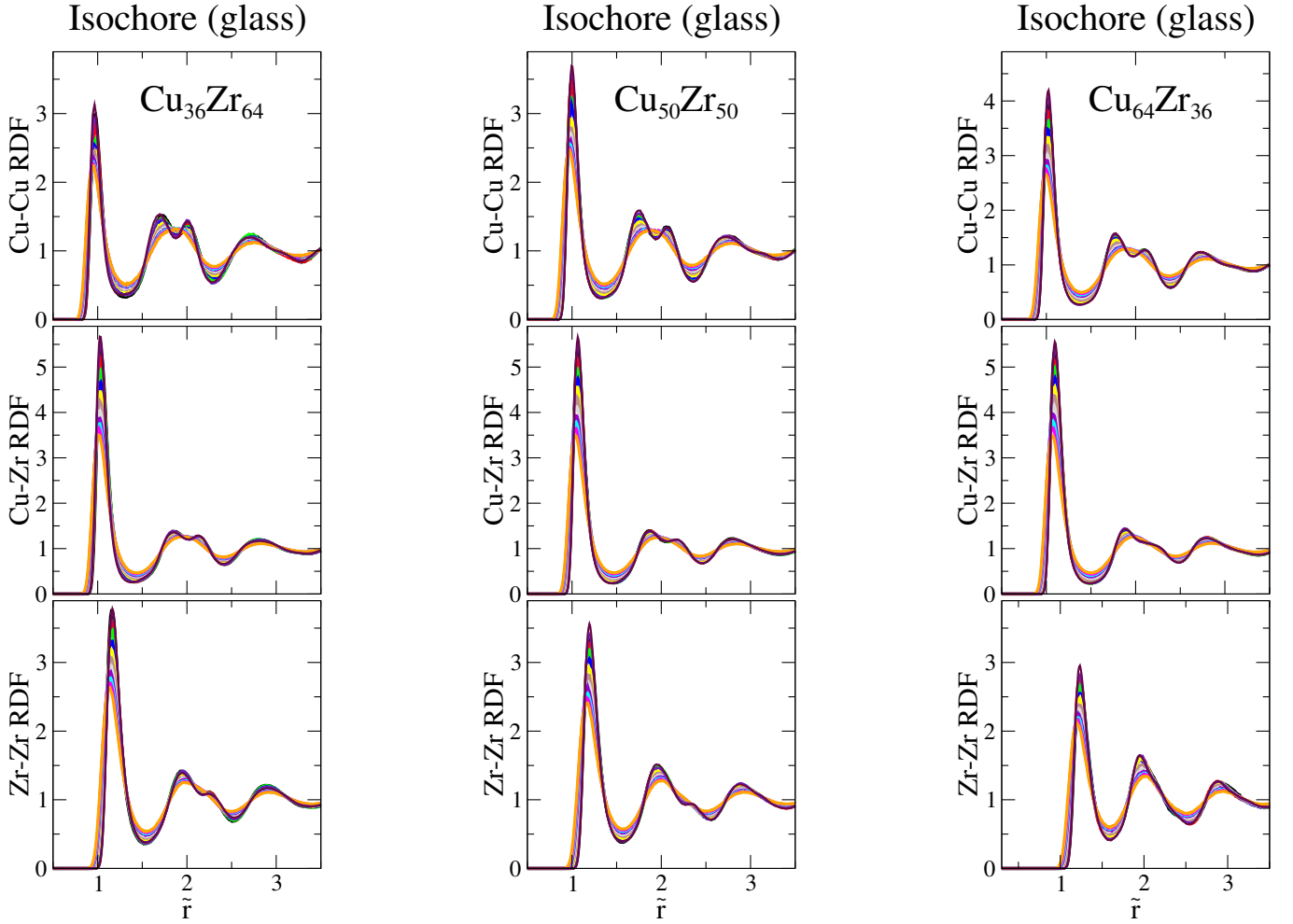


FIG. 10. Isochore glass-state RDFs, plotted as in Fig. 9. There is here a considerably larger variation of the structure.

$$B = \frac{-E_0\lambda^2}{12\pi s_0} \quad (16)$$

while the product $V_0(\beta\eta_2 - \kappa) = V_0\delta$ is determined from the shear modulus C_{44} via the expression

$$C_{44} = \frac{sV_0\delta\kappa}{8\pi s_0}. \quad (17)$$

Equation (16) and Eq. (17) are only correct in the nearest-neighbor approximation; Ref. 51 explains how to include more neighbors using a cutoff implemented via a Fermi function. The standard choice, which is used also in this work, corresponds to the edge of the Fermi function being between the 3rd and 4th neighbor shell of the equilibrium fcc crystal.

The above gives all parameters describing a pure metal. For two-component systems like CuZn mixtures, some generalization of the energy expression is required [51].

[1] A. L. Greer, “Metallic glasses,” *Science* **267**, 1947–1953 (1995).

[2] M. Zink, K. Samwer, W. L. Johnson, and S. G. Mayr, “Plastic deformation of metallic glasses: Size of shear transformation zones from molecular dynamics simulations,” *Phys. Rev. B* **73**, 172203 (2006).

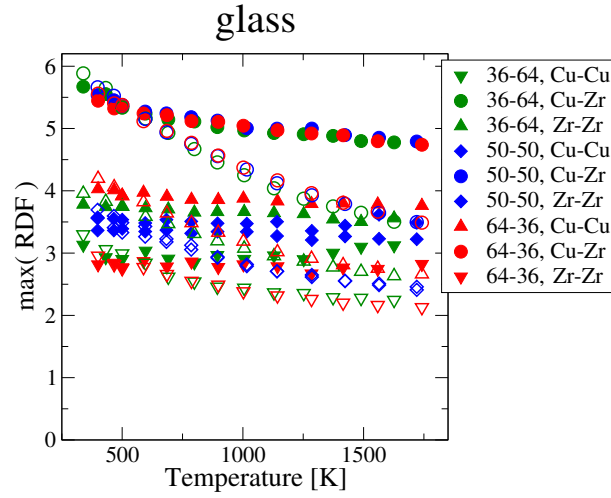


FIG. 11. Maximum values of all RDFs of Fig. 9 and Fig. 10, i.e., value of the RDF at the first peak. The full symbols represent isomorphs and the open symbols represent isochores. The isomorph values are not invariant, in particular for the Cu-Zr functions, but the general picture is that of significantly better invariance along the isomorphs than along isochores of same temperature variation.

- [3] M.I. Mendelev, M.J. Kramer, R.T. Ott, and D.J. Sordet, “Molecular dynamics simulation of diffusion in supercooled Cu–Zr alloys,” *Phil. Mag.* **89**, 109–126 (2009).
- [4] W. H. Wang, “The elastic properties, elastic models and elastic perspectives of metallic glasses,” *Prog. Mater. Sci.* **57**, 487–656 (2012).
- [5] W. H. Wang, “Dynamic relaxations and relaxation-property relationships in metallic glasses,” *Prog. Mater. Sci.* **106**, 100561 (2019).
- [6] M.-B. Tang, D.-Q. Zhao, M.-X. Pan, and W.-H. Wang, “Binary Cu-Zr bulk metallic glasses,” *Chinese Phys. Lett.* **21**, 901–903 (2004).
- [7] S. A. Rice and P. Gray, *The Statistical Mechanics of Simple Liquids* (Interscience, New York, 1965).
- [8] H. N. V. Temperley, J. S. Rowlinson, and G. S. Rushbrooke, *Physics of Simple Liquids* (Wiley, New York, 1968).
- [9] S. M. Stishov, “The Thermodynamics of Melting of Simple Substances,” *Sov. Phys. Usp.* **17**, 625–643 (1975).
- [10] J.-L. Barrat and J.-P. Hansen, *Basic Concepts for Simple and Complex Liquids* (Cambridge University Press, 2003).
- [11] T. S. Ingebrigtsen, T. B. Schröder, and J. C. Dyre, “What is a simple liquid?” *Phys. Rev. X* **2**, 011011 (2012).
- [12] J.-P. Hansen and I. R. McDonald, *Theory of Simple Liquids: With Applications to Soft Matter*, 4th ed. (Academic, New York, 2013).
- [13] J. O. Hirschfelder, C. F. Curtiss, and R. B. Bird, *Molecular Theory of Gases and Liquids* (John Wiley & Sons (New York), 1954).
- [14] J. D. Bernal, “The Bakerian lecture, 1962. The structure of liquids,” *Proc. R. Soc. London Ser. A* **280**, 299–322 (1964).
- [15] B. Widom, “Intermolecular forces and the nature of the liquid state,” *Science* **157**, 375–382 (1967).
- [16] J. A. Barker and D. Henderson, “What is “liquid”? Understanding the states of matter,” *Rev. Mod. Phys.* **48**, 587–671 (1976).
- [17] D. Chandler, J. D. Weeks, and H. C. Andersen, “Van der Waals picture of liquids, solids, and phase transformations,” *Science* **220**, 787–794 (1983).
- [18] J. C. Dyre, “Simple liquids’ quasiuniversality and the hard-sphere paradigm,” *J. Phys. Condens. Matter* **28**, 323001 (2016).
- [19] J. D. van der Waals, *Over de Continuïteit van den Gas- en Vloeistoftoestand* (Dissertation, University of Leiden, 1873).
- [20] J. S. Rowlinson, “The statistical mechanics of systems with steep intermolecular potentials,” *Mol. Phys.* **8**, 107–115 (1964).
- [21] D. Henderson and J. A. Barker, “Perturbation theory of fluids at high temperatures,” *Phys. Rev. A* **1**, 1266–1267 (1970).
- [22] H. C. Andersen, J. D. Weeks, and D. Chandler, “Relationship between the hard-sphere fluid and fluids with realistic repulsive forces,” *Phys. Rev. A* **4**, 1597–1607 (1971).
- [23] H. S. Kang, S. C. Lee, T. Ree, and F. H. Ree, “A perturbation theory of classical equilibrium fluids,” *J. Chem. Phys.* **82**, 414–423 (1985).
- [24] K. R. Harris, “The selfdiffusion coefficient and viscosity of the hard sphere fluid revisited: A comparison with experimental data for xenon, methane, ethene and trichloromethane,” *Molec. Phys.* **77**, 1153–1167 (1992).
- [25] J. E. Straub, “Analysis of the role of attractive forces in self-diffusion of a simple fluid,” *Molec. Phys.* **76**, 373–385 (1992).
- [26] D. Ben-Amotz and G. Stell, “Reformulation of Weeks–Chandler–Andersen perturbation theory directly in terms of a hard-sphere reference system,” *J. Phys. Chem. B* **108**, 6877–6882 (2004).
- [27] A. E. Nasrabad, “Thermodynamic and transport properties of the Weeks–Chandler–Andersen fluid: Theory and computer simulation,” *J. Chem. Phys.* **129**, 244508 (2008).
- [28] T. Rodriguez-Lopez, J. Moreno-Razo, and F. del Rio, “Thermodynamic scaling and corresponding states for the self-

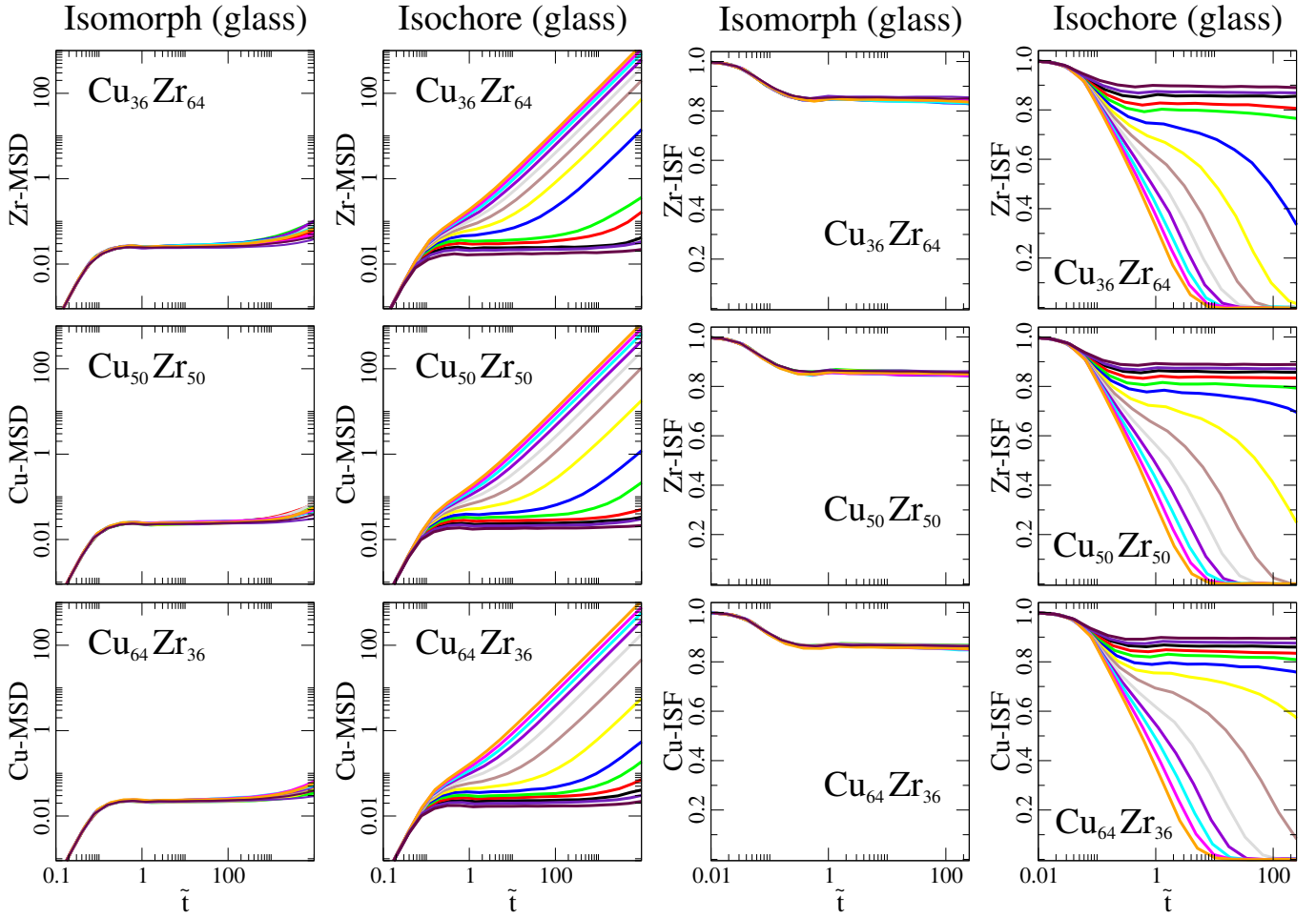


FIG. 12. Dynamics along the glass isomorphs and isochores of the glasses. The two left columns give data for the reduced MSD as a function of the reduced time. The two right columns give the analogous reduced-unit intermediate incoherent scattering function data, evaluated at the wave vector corresponding to the first peak of the corresponding RDF. Because the system is a glass, along the isomorphs the MSD is constant over a very long time and, correspondingly, the incoherent intermediate scattering function does not decay to zero. For the isochore state points, raising the temperature takes the system closer to a liquid with a MSD that at long times is proportional to time and an intermediate incoherent scattering function that decays to zero at long times. The overall picture is that, as for the liquid (Fig. 8), there is good isomorph invariance of the dynamics, but a significant variation along the isochores.

- diffusion coefficient of non-conformal soft-sphere fluids,” *J. Chem. Phys.* **138**, 114502 (2013).
- [29] Y. Rosenfeld, “Relation between the transport coefficients and the internal entropy of simple systems,” *Phys. Rev. A* **15**, 2545–2549 (1977).
- [30] J. C. Dyre, “Perspective: Excess-entropy scaling,” *J. Chem. Phys.* **149**, 210901 (2018).
- [31] D. Kivelson, G. Tarjus, X. Zhao, and S. A. Kivelson, “Fitting of viscosity: Distinguishing the temperature dependences predicted by various models of supercooled liquids,” *Phys. Rev. E* **53**, 751–758 (1996).
- [32] C. Alba-Simionesco, A. Cailliaux, A. Alegria, and G. Tarjus, “Scaling out the density dependence of the alpha relaxation in glass-forming polymers,” *Europhys. Lett.* **68**, 58–64 (2004).
- [33] C. M. Roland, S. Hensel-Bielowka, M. Paluch, and R. Casalini, “Supercooled dynamics of glass-forming liquids and polymers under hydrostatic pressure,” *Rep. Prog. Phys.* **68**, 1405–1478 (2005).
- [34] D. Gundermann, U. R. Pedersen, T. Hecksher, N. P. Bailey, B. Jakobsen, T. Christensen, N. B. Olsen, T. B. Schrøder, D. Fragiadakis, R. Casalini, C. M. Roland, J. C. Dyre, and K. Niss, “Predicting the density-scaling exponent of a glass-forming liquid from Prigogine–Defay ratio measurements,” *Nat. Phys.* **7**, 816–821 (2011).
- [35] E. R. Lopez, A. S. Pensado, J. Fernandez, and K. R. Harris, “On the Density Scaling of pVT Data and Transport Properties for Molecular and Ionic Liquids,” *J. Chem. Phys.* **136**, 214502 (2012).
- [36] K. Adrjanowicz, M. Paluch, and J. Pionteck, “Isochronal superposition and density scaling of the intermolecular dynamics in glass-forming liquids with varying hydrogen bonding propensity,” *RSC Adv.* **6**, 49370 (2016).
- [37] Y.-C. Hu, B.-S. Shang, P.-F. Guan, Y. Yang H.-Y. Bai, and W.-H. Wang, “Thermodynamic scaling of glassy dynamics

- and dynamic heterogeneities in metallic glass-forming liquid,” *J. Chem. Phys.* **145**, 104503 (2016).
- [38] C. M. Roland, R. Casalini, and M. Paluch, “Isochronal temperature–pressure superpositioning of the α -relaxation in type-A glass formers,” *Chem. Phys. Lett.* **367**, 259–264 (2003).
 - [39] K. L. Ngai, R. Casalini, S. Capaccioli, M. Paluch, and C. M. Roland, “Do theories of the glass transition, in which the structural relaxation time does not define the dispersion of the structural relaxation, need revision?” *J. Phys. Chem. B* **109**, 17356–17360 (2005).
 - [40] H. W. Hansen, A. Sanz, K. Adrjanowicz, B. Frick, and K. Niss, “Evidence of a one-dimensional thermodynamic phase diagram for simple glass-formers,” *Nat. Commun.* **9**, 518 (2018).
 - [41] T. B. Schröder and J. C. Dyre, “Simplicity of condensed matter at its core: Generic definition of a Roskilde-simple system,” *J. Chem. Phys.* **141**, 204502 (2014).
 - [42] N. Gnan, T. B. Schröder, U. R. Pedersen, N. P. Bailey, and J. C. Dyre, “Pressure-energy correlations in liquids. IV. “Isomorphs” in liquid phase diagrams,” *J. Chem. Phys.* **131**, 234504 (2009).
 - [43] J. C. Dyre, “Hidden scale envariance in condensed matter,” *J. Phys. Chem. B* **118**, 10007–10024 (2014).
 - [44] F. Hummel, G. Kresse, J. C. Dyre, and U. R. Pedersen, “Hidden scale invariance of metals,” *Phys. Rev. B* **92**, 174116 (2015).
 - [45] L. Friedeheim, J. C. Dyre, and N. P. Bailey, “Hidden scale invariance at high pressures in gold and five other face-centered-cubic metal crystals,” *Phys. Rev. E* **99**, 022142 (2019).
 - [46] R. Casalini and T. C. Ransom, “On the experimental determination of the repulsive component of the potential from high pressure measurements: What is special about twelve?” *J. Chem. Phys.* **151**, 194504 (2019).
 - [47] A. Sanz, T. Hecksher, H. W. Hansen, J. C. Dyre, K. Niss, and U. R. Pedersen, “Experimental evidence for a state-point-dependent density-scaling exponent of liquid dynamics,” *Phys. Rev. Lett.* **122**, 055501 (2019).
 - [48] R. Casalini and T. C. Ransom, “On the pressure dependence of the thermodynamical scaling exponent γ ,” *Soft Matter* **16**, 4625–4631 (2020).
 - [49] M. J. Puska, R. M. Nieminen, and M. Manninen, “Atoms embedded in an electron gas: Immersion energies,” *Phys. Rev. B* **24**, 3037–3047 (1981).
 - [50] J. K. Nørskov, “Covalent effects in the effective-medium theory of chemical binding: Hydrogen heats of solution in the 3d metals,” *Phys. Rev. B* **26**, 2875–2885 (1982).
 - [51] K. W. Jacobsen, P. Stoltze, and J. K. Nørskov, “A semi-empirical effective medium theory for metals and alloys,” *Surf. Sci.* **366**, 394–402 (1996).
 - [52] S. M. Foiles, M. I. Baskes, and M. S. Daw, “Embedded-atom-method functions for the fcc metals Cu, Ag, Au, Ni, Pd, Pt, and their alloys,” *Phys. Rev. B* **33**, 7983–7991 (1986).
 - [53] M. S. Daw, S. M. Foiles, and M. I. Baskes, “The embedded-atom method: a review of theory and applications,” *Mater. Sci. Rep.* **9**, 251–310 (1993).
 - [54] N. P. Bailey, T. S. Ingebrigtsen, J. S. Hansen, A. A. Veldhorst, L. Böhling, C. A. Lemarchand, A. E. Olsen, A. K. Bacher, L. Costigliola, U. R. Pedersen, H. Larsen, J. C. Dyre, and T. B. Schröder, “RUMD: A general purpose molecular dynamics package optimized to utilize GPU hardware down to a few thousand particles,” *Scipost Phys.* **3**, 038 (2017).
 - [55] K. W. Jacobsen, J. K. Nørskov, and M. J. Puska, “Interatomic interactions in the effective-medium theory,” *Phys. Rev. B* **35**, 7423–7442 (1987).
 - [56] J. K. Nørskov and N. D. Lang, “Effective-medium theory of chemical binding: Application to chemisorption,” *Phys. Rev. B* **21**, 2131–2136 (1980).
 - [57] A. Păduraru, A. Kenoufi, N. P. Bailey, and J. Schiøtz, “An interatomic potential for studying CuZr bulk metallic glasses,” *Adv. Eng. Mater.* **9**, 505–508 (2007).
 - [58] N. P. Bailey, U. R. Pedersen, N. Gnan, T. B. Schröder, and J. C. Dyre, “Pressure-energy correlations in liquids. I. Results from computer simulations,” *J. Chem. Phys.* **129**, 184507 (2008).
 - [59] E. Attia, J. C. Dyre, and U. R. Pedersen, “An extreme case of density scaling: The Weeks-Chandler-Andersen system at low temperatures,” *arXiv:2101.10663* (2021).
 - [60] L. Böhling, T. S. Ingebrigtsen, A. Grzybowski, M. Paluch, J. C. Dyre, and T. B. Schröder, “Scaling of viscous dynamics in simple liquids: Theory, simulation and experiment,” *New J. Phys.* **14**, 113035 (2012).
 - [61] T. S. Ingebrigtsen, L. Böhling, T. B. Schröder, and J. C. Dyre, “Thermodynamics of condensed matter with strong pressure-energy correlations,” *J. Chem. Phys.* **136**, 061102 (2012).
 - [62] D. M. Heyes, D. Dini, L. Costigliola, and J. C. Dyre, “Transport coefficients of the Lennard-Jones fluid close to the freezing line,” *J. Chem. Phys.* **151**, 204502 (2019).
 - [63] N. Chetty, K. Stokbro, K. W. Jacobsen, and J. K. Nørskov, “*Ab initio* potential for solids,” *Phys. Rev. B* **46**, 3798–3809 (1992).